Available online at www.sciencedirect.com
ScienceDirect
Journal of Catalysis 253 (2008) 57–65
JOURNAL OF CATALYSIS
www.elsevier.com/locate/jcat

Characterization and evaluation of Mo–V–Te–Nb mixed metal oxide catalysts fabricated via hydrothermal process with ultrasonic pretreatment for propane partial oxidation

Xiu-Juan Yang [a,b], Ru-Ming Feng [b], Wei-Jie Ji [b,*], Chak-Tong Au [a,*]

[a] *Department of Chemistry, Center for Surface Analysis and Research, Hong Kong Baptist University, Kowloon Tong, Hong Kong, China*
[b] *Key Laboratory of Mesoscopic Chemistry, Ministry of Education, School of Chemistry and Chemical Engineering, Nanjing University, Nanjing 210093, PR China*

Received 30 August 2007; revised 22 October 2007; accepted 22 October 2007

Available online 26 November 2007

Abstract

$Mo_{1.00}V_xTe_{0.20}Nb_{0.16}O_n$ ($x = 0.35$–0.50) mixed-metal oxide catalysts were synthesized through ultrasonic and hydrothermal treatments. Both TeO_2 and H_6TeO_6 were used as tellurium sources. The enhanced dispersion of TeO_2 by ultrasonic treatment is crucial for obtaining an active and selective Mo–V–Te–Nb–O catalyst for acrylic acid (AA) formation from propane oxidation. The TeO_2-derived $Mo_{1.00}V_xTe_{0.20}Nb_{0.16}O_n$ ($x = 0.35$–0.41) are superior to their H_6TeO_6-derived counterparts; propane conversion and AA selectivity over the $Mo_{1.00}V_{0.41}Te_{0.20}Nb_{0.16}O_n$ is 55% and 60 mol% at 380 °C, respectively, giving an AA formation rate of 22.3 μmol g^{-1} min^{-1}. Based on the physicochemical properties of the catalysts, we propose that the ultrasonic treatment can give rise to (i) enhanced presence of the orthorhombic $Te_2M_{20}O_{57}$ (M = Mo, V, Nb) and hexagonal $Te_{0.33}MO_{3.33}$ (M = Mo, V, Nb) phases, (ii) surface enrichment of Te, (iii) enhanced reactivity of lattice oxygen, (iv) an increase in Mo–O–Te and V–O–Te entities, and (v) better isolation of active sites.

Keywords: Propane; Acrylic acid; Mixed metal oxide; Ultrasonic treatment; Hydrothermal synthesis

1. Introduction

Due to the abundance and low cost of light alkanes, the selective oxidation of methane, ethane, propane, and butane to oxygenates has economic and environmental implications [1]. Acrylic acid (AA) is an important and versatile chemical used in the fabrication of absorbents, detergent, adhesives, and polymers [2]. The industrialized process for AA production involves two separate steps: the oxidation of propylene to acrolein and the oxidation of acrolein to AA. In view of the success in the direct oxidation of *n*-butane to maleic anhydride [3], the one-step oxidation of propane to AA has attracted increasing attention in recent years. Various catalyst systems have been studied, including vanadium phosphorus oxides (VPOs) [4,5], heteropolyacids (HPCs) [6–8], and mixed metal oxides (MMOs) [9–49]. Despite the fact that VPOs have been successfully industrialized in the oxidation of *n*-butane to maleic anhydride, the catalysts are not as effective in propane partial oxidation, because activation of the C–H bond of propane is more difficult than that of *n*-butane. The performance of HPCs for propane conversion to AA is unsatisfactory, and the poor thermal stability of HPCs limits their applications at elevated temperatures. So far, the catalyst systems considered the most likely candidates are the MMOs, especially the Mo–V–Te(Sb)–Nb–O initially proposed by Mitsubishi Chemicals for propane ammoxidation to acrylonitrile [10]. Nevertheless, significant variations in catalytic performance have been observed over the MMOs with apparently identical Mo–V–Te–Nb compositions, suggesting that there are intrinsic alterations in catalyst nature with different preparation approaches [11–17]. Catalyst structure and performance also have been found to be very sensitive to preparation history [11,12].

Among the various approaches, the hydrothermal method has been frequently used for the synthesis of active and stable

* Corresponding authors.
E-mail addresses: jiwj@nju.edu.cn (W.-J. Ji), pctau@hkbu.edu.hk (C.-T. Au).

0021-9517/$ – see front matter
doi:10.1016/j.jcat.2007.10.020

Table 1
Nominal, bulk, and surface elemental compositions (Mo/V/Te/Nb atomic ratios) of catalysts

Catalyst[a]	Nominal composition (adopted in preparation)	Bulk composition (measured by ICP)	Surface composition (measured by XPS)
A1	$Mo_{1.00}V_{0.35}Te_{0.20}Nb_{0.16}$	1.00/0.25/0.27/0.37	1.00/0.13/0.60/0.21
A2	$Mo_{1.00}V_{0.41}Te_{0.20}Nb_{0.16}$	1.00/0.29/0.27/0.37	1.00/0.14/0.53/0.24
A3	$Mo_{1.00}V_{0.50}Te_{0.20}Nb_{0.16}$	1.00/0.31/0.28/0.39	1.00/0.19/0.39/0.15
B1	$Mo_{1.00}V_{0.35}Te_{0.20}Nb_{0.16}$	1.00/0.28/0.27/0.37	1.00/0.15/0.56/0.24
B2	$Mo_{1.00}V_{0.41}Te_{0.20}Nb_{0.16}$	1.00/0.32/0.28/0.38	1.00/0.16/0.48/0.24
B3	$Mo_{1.00}V_{0.50}Te_{0.20}Nb_{0.16}$	1.00/0.32/0.25/0.35	1.00/0.16/0.45/0.18

[a] A1, A2, and A3 catalysts were prepared by using TeO_2 as Te source whereas B1, B2, and B3 catalysts were prepared by adopting H_6TeO_6 as Te source.

MMO catalysts [19–24]. In this article, we report the preparation of $Mo_{1.00}V_xTe_{0.20}Nb_{0.16}O_n$ ($x = 0.35$–0.50) via an improved methodology, namely ultrasonic pretreatment of TeO_2-containing suspension or H_6TeO_6-containing solution before the hydrothermal process. The generation as well as the performance of these catalysts has been found to be reproducible. The prepared catalysts were systematically characterized by inductively coupled plasma-atomic emission spectrometry (ICP-AES), X-ray diffraction (XRD), FT-IR, Raman, UV–vis diffuse reflectance spectroscopy (UV–vis DRS), X-ray photoelectron spectroscopy (XPS), high-resolution transmission electron microscopy (HRTEM), H_2 temperature-programmed reduction (H_2-TPR), and NH_3-calorimetric measurement. The aim of the study is to explore the crucial parameters for catalyst fabrication that would affect the characteristics and, consequently, the activity of the catalysts.

2. Experimental

2.1. Catalyst preparation

The raw materials were purchased from Aldrich Chemical Company, Ltd. and used without further treatment. For the preparation of the $Mo_{1.00}V_xTe_{0.20}Nb_{0.16}O_n$ catalysts, the typical preparation process is as follows: 4.50 g ammonium paramolybdate was dissolved in 20 ml deionized (DI) water under stirring at room temperature (RT) to form a solution; then 0.81 g of TeO_2 powder or 1.16 g of telluric acid was added. According to the specific nominal elemental composition of a sample, an appropriate amount of vanadyl sulfate (H_2O content determined by TG measurement) was dissolved in 10 ml of DI water at RT to form a deep-blue solution, which was added dropwise into the aqueous Mo–Te mixture under stirring. At the final stage, a solution of 1.83 g of ammonium niobium oxalate dissolved in 20 ml of water was slowly added into the above Mo–V–Te mixture. To achieve better interaction of TeO_2 or telluric acid with the other component(s) in the preparation medium, the Mo–Te mixture (before the addition of vanadyl sulfate), as well as the as-generated mixture after the addition of ammonium niobium oxalate, were subjected to 45 min of ultrasonic treatment (80 W at 40 kHz; KQ 2200 DE, Kuen Shan Ultrasonic Instrument Co., Ltd., China). Then the resulting mixture was hydrothermally treated at 175 °C for 72 h in a Teflon-lined stainless steel autoclave. The solid thus obtained was filtered out, rinsed with DI water, and dried at 80 °C overnight to generate the "precursor," which was activated in a covered quartz crucible in an argon atmosphere at 600 °C for 2 h. The resulting solid was ground, pressed, crushed, and sieved to 20–40 mesh for use. Overall, six catalysts (A1, A2, A3, B1, B2, and B3) were prepared, as listed in Table 1. The A1, A2, and A3 catalysts were prepared using TeO_2 as the Te source, whereas the B1, B2, and B3 catalysts were prepared using H_6TeO_6. The A2† and B3† catalysts were prepared similarly to the A2 and B3 catalysts but without the ultrasonic treatment.

2.2. Catalyst characterization

The as-prepared and used catalysts were characterized by various techniques. The ICP-AES results were obtained on a J-A1100 instrument. The specific surface (BET) area of the samples was measured on a NOVA1200 apparatus with N_2 adsorption at 77 K. The phase composition of the samples was identified by powder XRD using an X′ TRA X-ray diffractometer (Cu$K\alpha$ radiation) in the 2θ range of 3°–60°. The FT-IR spectra of the catalysts were recorded using a NEXUS-870 FT-IR spectrometer at RT. The UV–vis diffuse reflectance spectra were recorded at RT using a Shimadzu UV-2401PC spectrometer, using barium sulfate as the reference compound. The Raman spectra were collected over a Renishaw Raman microscope with a laser source of 514 nm. XPS investigation was performed on a VG ESCALAB MK II spectrometer using Mg$K\alpha$ radiation with a 12-kV high-voltage and a 20-mA emission current. The surface elemental composition was estimated based on the corresponding peak areas normalized with reference to the Wagner factor database. The V $2p_{3/2}$, Mo $3d_{5/2}$, Nb $3d_{5/2}$, Te $3d_{5/2}$, and O 1s binding energies (BEs) were calibrated against the C 1s BE (284.6 eV) of the contaminant carbon. The HRTEM images were obtained using an FEI Tecnai G^2 20 S-twin transmission electron microscope. H_2-TPR was carried out in the temperature range of RT to 800 °C. The sample was reduced in a flow of 5% H_2/Ar (40 ml/min) at a heating rate of 5 °C/min. NH_3-calorimetric measurement was performed on a Tian-Calvet heat-flux apparatus; the sample was degassed at 300 °C for 1 h before being exposed to ammonia.

2.3. Catalytic evaluation

Propane partial oxidation was carried out at atmospheric pressure in a conventional fixed-bed Pyrex tubular reactor

(8 mm i.d.) at 360–420 °C. The feed composition was $C_3H_8/O_2/H_2O/He = 6/12/40/42$ (volume ratio), and the total gas hourly space velocity (GHSV) was 1500 ml/(h g_{cat}). The reaction products were analyzed by two online gas chromatographs using a HP FFAP capillary column (0.32 mm × 25 m) for separation of propane and oxygenates; a packed Alltech Hayesep D column (100/120 mesh, 1/8′ × 4 m) for separation of O_2 (CO), CO_2, $C_3^=$ and C_3; and a packed 5A molecular sieve column (80/100 mesh, 1/8′ × 2 m) for separation of O_2 and CO.

3. Results

3.1. Catalyst characterization

3.1.1. Bulk and surface composition

As shown in Table 1, the bulk (measured by ICP) and surface (measured by XPS) elemental compositions differed from the nominal values adopted for catalyst preparation. This suggests that some of the constituent elements were lost (mostly the Mo and V elements). The table also shows that the surfaces were enriched with Te but depleted with V. It is noteworthy that the Te enrichment on the surfaces of the catalysts prepared hydrothermally without ultrasonic pretreatment was insignificant. We propose that ultrasonic treatment could enrich the surfaces of the $Mo_{1.00}V_xTe_{0.20}Nb_{0.16}O_n$ catalysts with Te.

3.1.2. XRD

Two phases have been proposed to exist in the MMO-type catalysts. The orthorhombic phase (denoted as M1) is responsible for propane activation and propylene formation, whereas the hexagonal phase (denoted as M2) is active and selective for AA generation [17,25–27]. The XRD patterns (Fig. 1) of the $Mo_{1.00}V_xTe_{0.20}Nb_{0.16}O_n$ catalysts exhibited major diffraction peaks at $2\theta = 6.6°$, 7.7°, 9.0°, 22.1°, 26.6°, 27.2°, 28.3°, and 45.2°, attributable to the orthorhombic $Te_2M_{20}O_{57}$ (M = Mo, V, Nb) phase (M1) [28]. The peaks at $2\theta = 22.1°$, 28.2°, 36.2°, 44.7°, and 50.0° can be ascribed to the hexagonal $Te_{0.33}MO_{3.33}$ (M = Mo, V, Nb) phase (M2) [30]. The catalysts prepared with ultrasonic treatment demonstrated greater amounts of the M2 phase (A2 vs A2† and B3 vs B3†). Furthermore, the diffraction peaks at $2\theta = 12.7°$, 23.3°, 25.6°, 27.2°, and 38.9° can be ascribed to the MoO_3 (MoO_x) phase. The catalysts prepared with ultrasonic treatment demonstrated smaller amounts of the MoO_3 (MoO_x) phase. In view of the complexity of the XRD patterns, it is difficult to exclude the possibility that minute amounts of the (V, Nb)-substituted Mo_5O_{14} and $TeMo_5O_{16}$ phases were present in the catalysts.

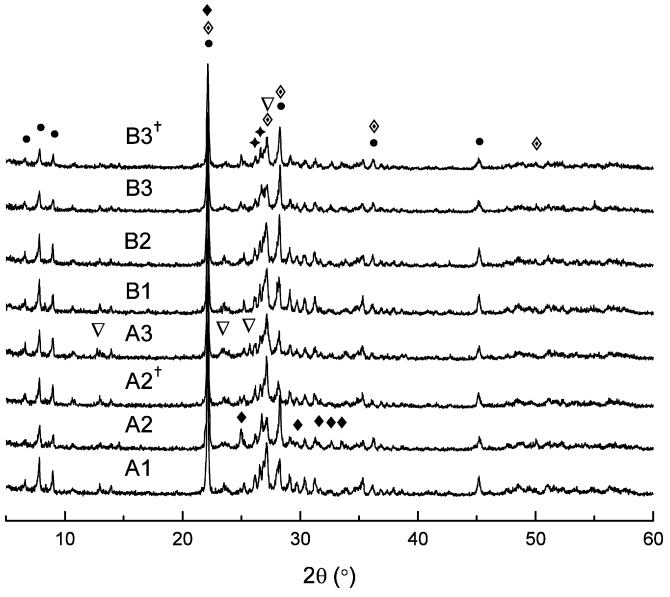

Fig. 1. X-ray diffraction patterns of $Mo_{1.00}V_xTe_{0.20}Nb_{0.16}O_n$ ($x = 0.35$–0.50) catalysts. The A2† and B3† samples were prepared in a way similar to that of A2 and B3 but without ultrasonic treatment. (●) $Te_2M_{20}O_{57}$ (M = Mo, V, Nb), (◈) $Te_{0.33}MO_{3.33}$ (M = Mo, V, Nb), (▽) MoO_3/MoO_x, (✦) $TeMo_5O_{16}$, (◆) (V, Nb)-substituted Mo_5O_{14}.

3.1.3. FT-IR

The FT-IR spectra of the catalysts are shown in Fig. 2. The IR band in the range of 900–1000 cm^{-1} is related to the symmetric stretching vibration of the Mo=O group. With an increasing V content, the ca. 910 cm^{-1} band decreased in intensity. The characteristic bands (that at 990 cm^{-1} together with a weak band at 818 cm^{-1}) of Mo=O vibration in free MoO_3 [31] were weak, suggesting a low amount of free MoO_3 in the samples prepared with ultrasonic treatment. The bands in the 700–900 cm^{-1} region can be ascribed to the antisymmetric vibrations of Mo–O–M (M = Mo, Te, Nb). The band at 882 cm^{-1} declined in intensity with increasing V content as a result of Mo substitution by V in Mo–O–M. The band at 636 cm^{-1} is due to the Te–O bond [32] and is hardly influenced by the change in V content. In addition, the bands at ca. 590 and 455 cm^{-1} can be attributed to the V–O–M (M = Mo, V) species [14]. The species detected by FT-IR are coincident with the phases observed in XRD examination.

3.1.4. Raman and UV–vis DRS

Raman spectra provide information on the vibration property and local structure of the MMO catalysts. Fig. 3 shows a

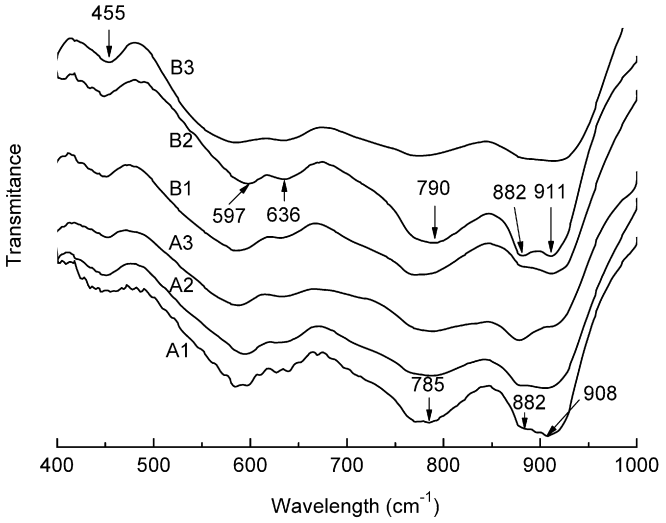

Fig. 2. FT-IR spectra of $Mo_{1.00}V_xTe_{0.20}Nb_{0.16}O_n$ ($x = 0.35$–0.50) catalysts.

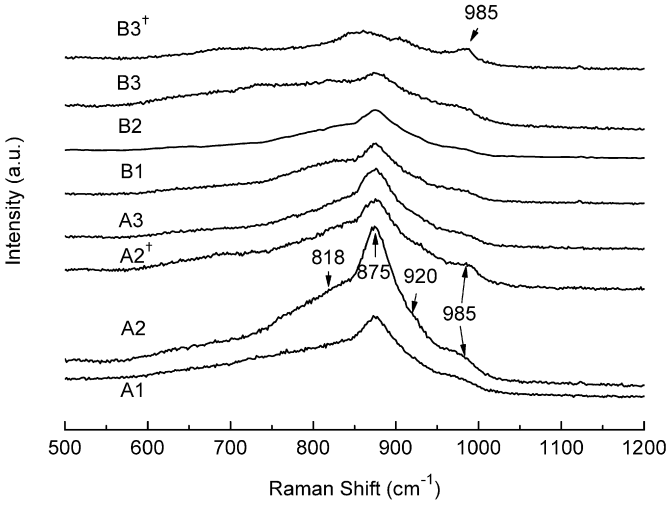

Fig. 3. Raman spectra of $Mo_{1.00}V_xTe_{0.20}Nb_{0.16}O_n$ ($x = 0.35$–0.50) catalysts.

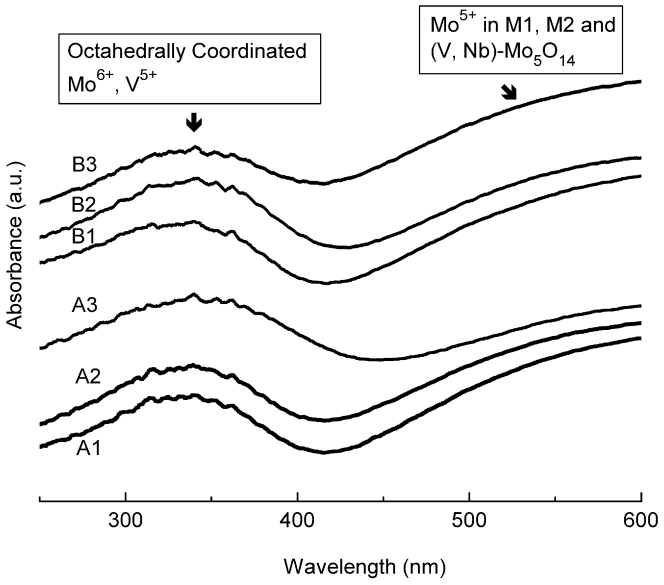

Fig. 4. Diffuse reflectance UV–vis spectra of $Mo_{1.00}V_xTe_{0.20}Nb_{0.16}O_n$ ($x = 0.35$–0.50) catalysts.

broad band at ca. 875 cm^{-1} attributable to the stretching mode of bridging Mo–O–*M* bonds (*M* = Mo, V, and Nb) in polycrystalline MMOs [9]. The figure also shows that the 875-cm^{-1} band of the A2 and B3 samples were of higher intensity than the A2† and B3† samples, respectively. The shoulder at ca. 920 cm^{-1} is attributable to the Mo_5O_{14}-type structure, and the band at 985 cm^{-1} can be ascribed to MoO_3 or MoO_x oxide [33,34]. Compared with the A2† and B3† samples, the A2 and B3 samples exhibited a 985-cm^{-1} band of lower intensity, implying that the former contained greater amounts of MoO_3 or MoO_x oxide. The results are in agreement with those of the IR observations, in that the A2 and B3 samples had a low MoO_3 or MoO_x content. The broad bands at ca. 970 and 818 cm^{-1} likely are due to the V=O and V–O–*M* (*M* = Mo, V and Nb) species, respectively [31], and the presence of these two bands suggests the possible existence of the (V, Nb)-substituted Mo_5O_{14} entities.

UV–vis DRS is a useful technique for probing the electronic/coordination structure of MMOs. The broad band in the range of 250–450 nm (Fig. 4) indicates the presence of octahedrally coordinated Mo^{6+} and V^{5+} cations in the samples [20,21]. The significant band broadening of the A3 catalyst implies the presence of structural distortion. The broad band beyond 450 nm may be assigned to the Mo species with an oxidation state below +6 [35]. Asakura et al. [17] and Gaffney et al. [18] have reported that the presence of the partially reduced Mo species is important for propane activation. According to the results of our previous electron spin resonance investigation (not shown here), the concentration of Mo^{5+} in the M1 and M2 phases can be enhanced by the applied ultrasonic treatment.

3.1.5. XPS

We performed XPS analysis to determine the oxidation state of the constituent elements of the freshly activated and used catalysts. The results are summarized in Table 2. The Mo $3d_{5/2}$ BE was in the range of 232.3–232.6 eV, indicating that most of the Mo species had an oxidation number of +6. (The $3d_{5/2}$ BE of Mo^{5+} was 231.5 eV, whereas that of Mo^{6+} was 232.6 eV [18].)

Table 2
Mo $3d_{5/2}$, V $2p_{3/2}$, Te $3d_{5/2}$, Nb $3d_{5/2}$, and O 1s binding energies (eV) of catalysts

Catalyst	Mo $3d_{5/2}$	V $2p_{3/2}$	Te $3d_{5/2}$	Nb $3d_{5/2}$	O 1s
A1	232.5	516.4	576.2	206.7	530.2
A2	232.6	516.6	576.3	206.8	530.4
A2*[a]	232.5	516.2	576.3	206.9	530.3
A3	232.6	516.4	576.3	206.8	530.3
B1	232.5	516.2	576.2	206.6	530.2
B2	232.6	516.5	576.2	206.8	530.3
B3	232.3	516.2	576.0	206.5	530.2
B3*[a]	232.4	515.9	576.0	206.7	530.2

[a] A2* and B3* are used A2 and B3 catalysts, respectively.

The $3d_{5/2}$ BE of Te in all of the samples was ca. 576.2 eV, whereas that of Te in H_6TeO_6 was ca. 577.3 eV [36], suggesting that the oxidation number of the Te species was essentially +4. It also was found that the oxidation state of the Te constituent (retained as +4) was independent of the Te source used for catalyst fabrication. Janssen reported that high-temperature calcination of sample in an inert atmosphere could result in a change of the Te oxidation state from +6 to +4 [37]. We envisage that Te^{6+} could convert to Te^{4+} when the precursors were activated in static argon at 600 °C. The $3d_{5/2}$ BE of the Nb component of ca. 206.6 eV indicates an oxidation state of +5 [38]. The V $2p_{3/2}$ BE of the MMO catalysts of 516–517 eV suggests an oxidation state of 5^+. No significant change in the BE of the elements was seen before and after reaction (A2 vs A2* and B3 vs B3*), indicating that the oxidation states of the elements were essentially retained during the reaction.

3.1.6. H_2-TPR

Fig. 5 shows the H_2-TPR profiles of the samples. One broad peak in the range of 460–530 °C can be observed, due to the reduction of Mo^{6+}, V^{5+}, and Te^{4+} species. It is known that the Mo^{6+} and V^{5+} are reduced more easily in MMO solid solution

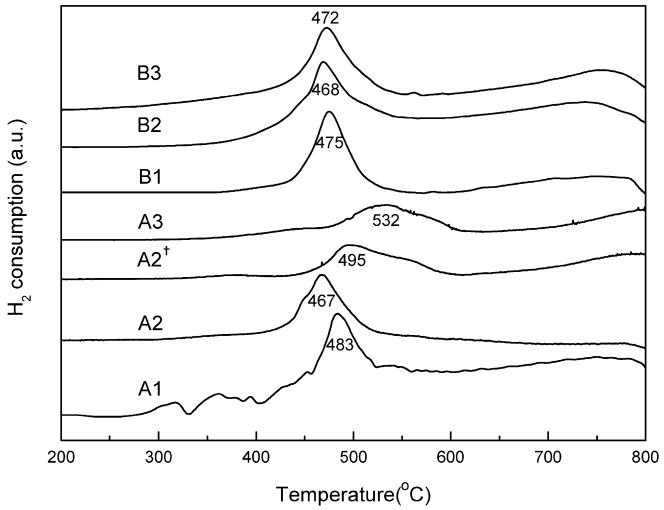

Fig. 5. H_2-TPR profiles of $Mo_{1.00}V_xTe_{0.20}Nb_{0.16}O_n$ ($x = 0.35$–0.50) catalysts.

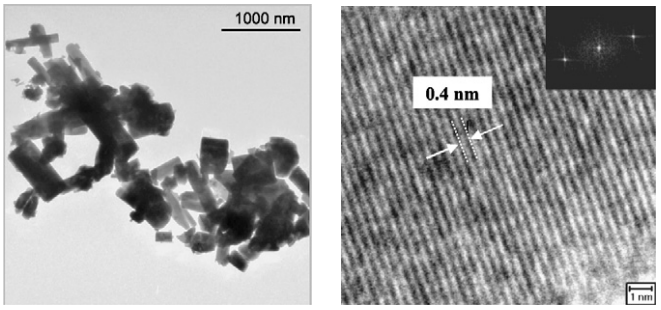

(a) (b)

Fig. 6. HRTEM images of (a) A2 and (b) B3 catalysts. (The inset is the selected area electron diffraction pattern of sample B3.)

than in pure MoO_3 and V_2O_5 [39]. The A2 sample exhibited the greatest reducibility of lattice oxygen, whereas A3 was the most difficult sample to reduce. The relatively higher temperature reduction peak of the A2† sample implies that ultrasonic treatment could result in the catalyst with enhanced reactivity of lattice oxygen. The change in reduction behavior was not apparent across the B-serial catalysts. The results demonstrate that when TeO_2 was used as the Te source, changing the V content had a significant effect on both the reactivity and reducibility of lattice oxygen, whereas this was not the case for the H_6TeO_6-derived catalysts.

3.1.7. HRTEM

The size and morphology of the MMO catalysts were examined by HRTEM; representative results for the A2 and B3 catalysts are shown in Fig. 6. Fig. 6a shows prism morphology with particle dimensions of several hundreds of nanometers; such prism-like morphology is commonly observed over the A and B serial catalysts. To enhance catalyst activity, Oshikara et al. [15] used grinding of activated catalyst to enlarge the cross-sectional exposure of prism particles. The adoption of ultrasonic treatment in catalyst preparation resulted in significantly reduced catalyst dimensions and enhanced exposure of the active planes. The HRTEM image and selected area electron

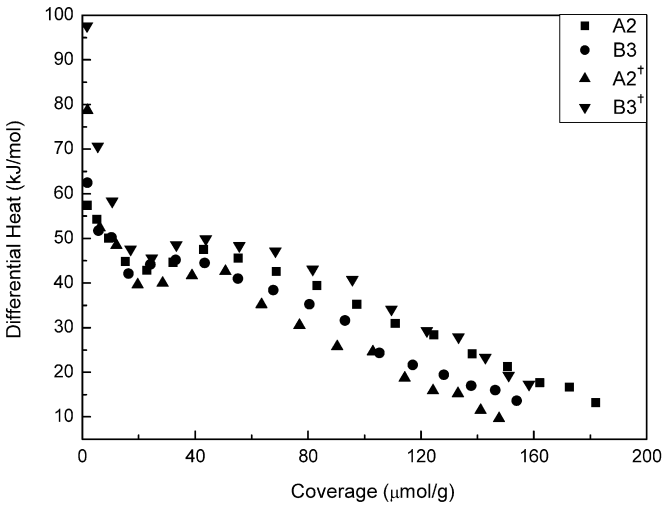

Fig. 7. Differential adsorption heat of NH_3 versus coverage over catalysts A2, A2†, B3, and B3†.

diffraction pattern of the B3 sample (Fig. 6b) reveal that the distance between the two neighboring atomic planes was 0.4 nm, in agreement with the d-value of the M1 phase as well as that of the M2 or Mo_5O_{14} phase. Because the catalysts are dominated by the M1 and M2 phases, the planes of Fig. 6b belong to either the M1 or M2 phase.

3.1.8. NH_3-calorimetric measurement

Surface acidity is known to affect the catalytic performance of MMO catalysts in propane partial oxidation [31]. Calorimetric measurement of the NH_3 probe was performed to monitor the surface acidity of the fabricated catalysts; results for catalysts A2, A2†, B3, and B3† are shown in Fig. 7. It can be seen that the initial adsorption heat of the A2 and B3 samples was lower than that of A2† and B3†; in other words, A2 and B3 had a lower surface acidity than A2† and B3†. On the other hand, because the NH_3 molecules can enter the empty channels of the M1 phase at high NH_3 coverage, the measured NH_3 coverage may reflect the amount of M1 phase in the samples. Accordingly, the A2 catalyst appears to have the highest M1 phase content in terms of the corresponding NH_3 coverage.

3.2. Catalytic activity

Table 3 presents the propane conversion and product distribution over the catalysts at 380 °C. The major products were AA, propylene, acetic acid, and carbon oxides (CO_x), similar to those detected by other researchers over this type of catalyst [14]. In terms of catalytic performance, A2 was the best among the TeO_2-derived MMO catalysts, whereas B3 was the best among the H_6TeO_6-derived catalysts. Among all of the catalysts, A2 was the most active and B3† the least active (Table 3). Compared with the A2 and B3 catalysts, the A2† and B3† catalysts prepared without ultrasonic treatment showed lower propane conversion and higher selectivity to propylene. These findings can be interpreted to indicate that the ultrasonic treatment enhanced the presence of the M2 phase at the expense of the MoO_3 (MoO_x) phase in the A2 and B3 catalysts.

Table 3
Reaction performance over catalysts at 380 °C[a]

Catalyst	BET (m^2/g)	Conversion (%)	Selectivity (mol%)					AA yield (mol%)	Rate of AA ($\mu mol\ g^{-1}\ min^{-1}$)
			AA	ACR[b]	AcOH[c]	C_3H_6	CO_x		
A1	5.2	37.2	65.2	0.1	1.7	7.4	25.6	24.2	16.2
A2	7.1	55.7	59.9	0.3	3.0	7.9	29.0	33.4	22.3
A2†[d]	3.2	29.7	65.9	0.5	5.0	12.4	16.2	19.6	13.2
A3	4.2	33.9	59.8	0.6	6.8	10.1	22.8	20.2	13.5
B1	5.6	42.9	38.7	0.2	2.6	14.4	44.1	16.6	11.2
B2	6.1	56.3	43.8	0.2	2.9	6.8	46.3	24.7	16.5
B3	7.0	51.0	54.3	0.1	3.6	5.9	36.2	27.7	18.5
B3†[d]	6.4	42.2	32.1	0.8	3.4	15.6	48.1	13.5	9.0

[a] Feed composition was C_3H_8/O_2/steam/He = 6/12/40/42 (v/v/v/v) with W/F = 249 g_{cat} h (mol C_3H_8)$^{-1}$.
[b] ACR: acrolein.
[c] AcOH: acetic acid.
[d] A2† [49] and B3† were prepared in a way similar to that of A2 and B3 but without ultrasonic treatment.

In the current study, we adopted a feed composition of $C_3H_8/O_2/H_2O$/He = 6/12/40/42 (volume ratio). The presence of water is known to play an important role in propane partial oxidation and can facilitate the formation of AA [40,41]. Novakova et al. pointed out that water vapor enhances the formation of oxygenates by sustaining the active sites in a partially reduced state [23]. The presence of steam causes a decline in propane conversion but an increase in AA selectivity by restraining CO_x formation. We have found that a 40 vol% of steam provides optimal performance. Table 3 shows that the yield of AA over the A or B serial catalysts appears to be correlated with the catalysts' specific surface areas. The findings demonstrate that ultrasonic pretreatment can enhance a catalyst's surface area by reducing the particle size; this is also supported by the results of HRTEM observation (Fig. 6). Therefore, the catalytic activity of A2 was much greater than that of A2† on the basis of per unit mass of catalyst, a finding that is meaningful for practical applications. On the other hand, the catalytic activity on the basis of per unit surface area of catalyst appeared to be rather similar across the A-serial catalysts, with that of A2 lying between that of A1 and A3. These findings suggest that the number of active sites is not proportional to the increase in surface area. In terms of turnover rate of AA (TOR_{AA}), the A-serial catalysts were more active than the B-serial catalysts (Fig. 8). Moreover, the A-serial catalysts exhibited similar activity when the surface V/(Mo + V + Te + Nb) ratio was varied from 0.065 to 0.11, whereas the B-serial catalysts showed a significant increase in activity when the surface V/(Mo + V + Te + Nb) ratio was changed from 0.077 to 0.085 (Fig. 8).

Figs. 9 and 10 show that propane conversion over A2 first increased from 41 to 70% as the temperature was raised from 360 to 400 °C, then declined slightly to 68% at 420 °C. In a temperature range of 360–420 °C, the selectivity of CO_x increased from 14 to 78%, whereas that of AA declined from 66 to 12%. In the meantime, the selectivity of propylene decreased gradually, and that of acetic acid remained low. Fig. 10 shows that an AA yield of 33.4 mol% could be achieved over the A2 catalyst at 380 °C. Above 400 °C, the deep oxidation of propylene and oxygenated compounds became dominant, and the selectivity of AA, propylene, and acetic acid declined. As shown in

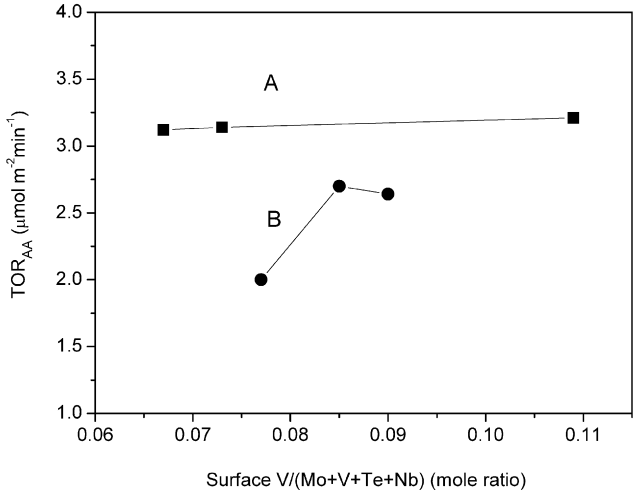

Fig. 8. TOR_{AA} versus surface V/(Mo + V + Te + Nb) mole ratio across the A and B serial catalysts.

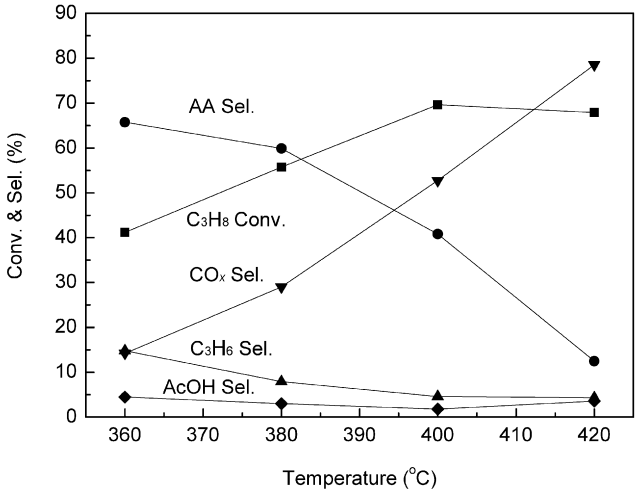

Fig. 9. Temperature dependence of catalyst performance of A2. GHSV = 1500 ml/(h g_{cat}), feed composition: $C_3H_8/O_2/H_2O$/He = 6/12/40/42 (volume ratio).

Fig. 11, the used (ca. 40 h of running) and unused A2 catalysts display similar XRD patterns. The $Mo_{1.00}V_xTe_{0.20}Nb_{0.16}O_n$ catalysts prepared by adopting the ultrasonic and hydrothermal

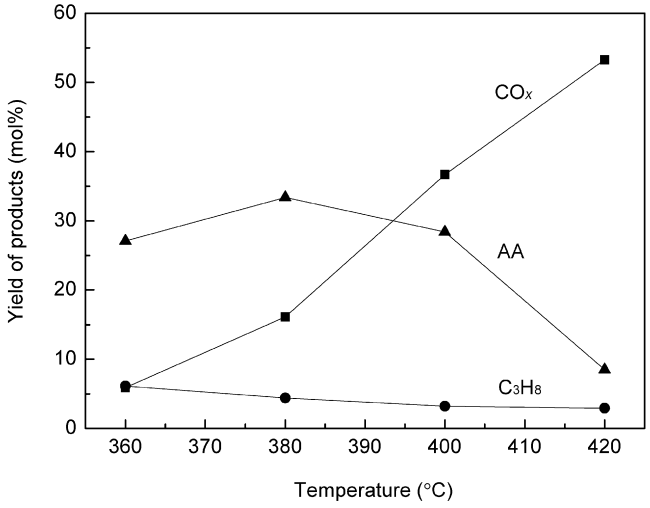

Fig. 10. Yield of AA, CO_x, and C_3H_6 versus reaction temperature over catalyst A2. GHSV = 1500 ml/(h g_{cat}), $C_3H_8/O_2/H_2O/He$ = 6/12/40/42 (volume ratio).

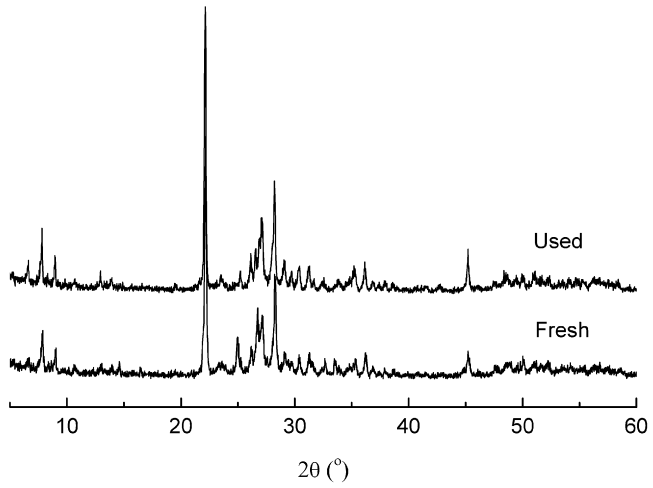

Fig. 11. XRD patterns of the A2 catalyst acquired before and after reaction.

treatments are structurally stable. Fig. 12 plots the selectivity of the main products with respect to propane conversion over the A2 catalyst. The figure shows decreasing selectivity to AA and propylene with increasing propane conversion, due to CO_x formation.

4. Discussion

4.1. Phase composition

The elemental constitution, phase composition, redox property, and surface acidity of the MMO catalysts have been found to be sensitive to the method of catalyst fabrication. Previous studies [17,25] demonstrated that catalyst performance can be related to the M1 and M2 phases. As reported by Ueda et al., hexagonal, pentagonal and heptagonal channels are present in the M1 phase; the Te species are located in the distorted hexagonal channels, and the niobium species are accommodated in the pentagonal bipyramids of MO_7 (M = Mo, V) [43,44]. In the

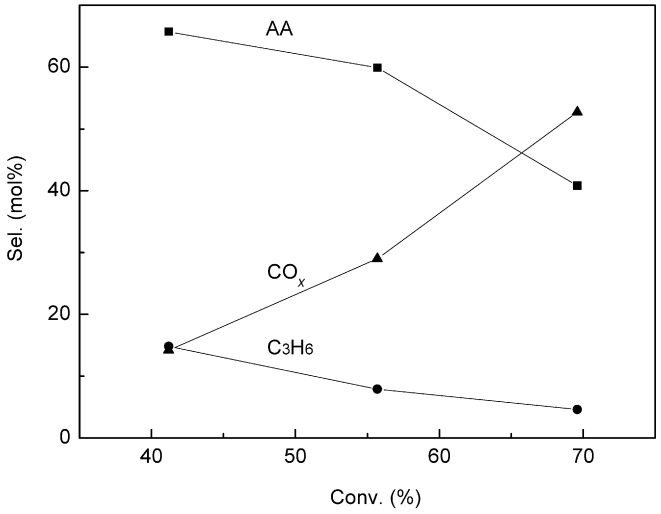

Fig. 12. Product distribution versus propane conversion over catalyst A2.

M2 phase, the hexagonal channels are occupied by tellurium species. The stoichiometry of the orthorhombic and hexagonal phases is $Te_2M_{20}O_{57}$ and $Te_{0.33}MO_{0.33}$ (M = Mo, V, Nb), respectively. The synergism effect between the M1 and M2 phases was suggested by Ushikubo et al. [25] and further studied by Baca et al. [27]. Millet et al. proposed the tellurite entities of trigonal bipyramid (TeO_4E) in the hexagonal phase and the distorted trigonal pyramid (TeO_3E) in the orthorhombic phase [28], and the hexagonal phase (M2) is considered to be the tellurium reservoir for the M1 phase [29]. The $Te_2M_{20}O_{57}$ phase is vital for the oxidative activation of propane to propylene, and the $Te_{0.33}MO_{3.33}$ phase, containing higher concentrations of Te^{4+}, plays an important role in the conversion of propylene to AA. A synergism of thoroughly mixed M1 and M2 in microscale (<5 μm) contact also was proposed by Grasselli [45]. In an active and selective MMO catalyst, the M1 and M2 phases are usually dominant, whereas the (V, Nb)-substituted Mo_5O_{14} and MoO_3 phases are minor. The results of the present study reveal that with the application of ultrasonic treatment, the formation of the M1 and particularly the M2 phase was enhanced at the expense of the MoO_3/MoO_x phase, and the TeO_2-derived Mo–V–Te–Nb catalyst can outperform the H_6TeO_6-derived one. This finding has never been reported until now.

4.2. Reaction mechanism and effect of ultrasonic treatment

Vitry et al. [46] pointed out that the AA formation rate in propane partial oxidation is first order in propane and is almost independent of O_2 partial pressure. They suggested that the activation and cleavage of the propane C–H bond is a rate-determining step. Scheme 1 depicts the reaction network of propane oxidation as illustrated by Botella et al. [14]. AA is generated through the acrolein intermediate while acetic acid is produced via acetone. In both cases, propylene is the intermediate of acrolein and acetone generation. Grasselli et al. [47] suggested that (i) propane is activated and converted to propylene on the V-sites ($V^{5+}{=}O \rightleftarrows V^{\bullet 4+}{-}O^{\bullet}$), (ii) the oxidation of

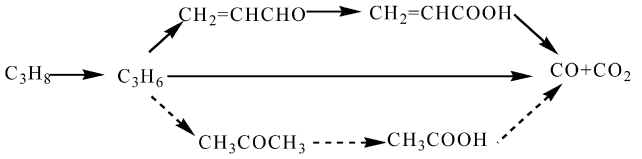

Scheme 1. Reaction network for the propane partial oxidation over Mo–V–Te–(Nb) catalysts [14].

propylene occurs on the Mo/Te sites, and (iii) the oxidation of acrolein to AA occurs on the Mo/Nb sites [48]. The function of the Te^{4+} sites for the abstraction of an allylic hydrogen (α-H) from propylene was first proposed by Millet et al. [28] and Grasselli [45], whereas that of Mo^{6+} sites for oxygen-insertion into the π-allylic intermediates was suggested by Grasselli [45]. Application of ultrasonic treatment in catalyst fabrication enhanced the dispersion of the Te constituent and, consequently, the presence of Te on the surface (Table 1); such a situation is considered beneficial for AA formation.

As suggested by Grasselli [45], the overoxidation of products on MMO catalysts can be suppressed by having the active sites spatially isolated by the Nb species. According to Ueda et al. [43,44], the Nb species can promote rapid desorption of the desired products so as to prevent further oxidation. The ultrasonic treatment adopted after the addition of Nb during catalyst fabrication can enhance the interaction of Nb with the other constituents, leading to increased site isolation. In addition, the enhanced dispersion of Nb species also can lead to shorter prism particles (Fig. 6a) and better exposure of the active (100) plane [27,31,49]. Guliants et al. [22] measured the consumption rate of propane and the formation rate of propylene and AA, and found that these rates were dependent on the surface concentration of V rather than on that of Mo and Te (as determined by low-energy ion scattering). We observed that within a certain range of overall surface V concentration (as determined by XPS), the TOR_{AA} increased with a rise in surface V content over the H_6TeO_6-derived catalysts, whereas the TOR_{AA} remained almost unchanged over the TeO_2-derived catalysts (Fig. 8). Védrine et al. suggested that the acid sites of medium strength in high density are responsible for good catalytic performance [31]. The results of NH_3 calorimetric measurement revealed that catalysts A2 and B3 displayed surface acidity of relatively milder strength (Fig. 7). Clearly, catalyst surface acidity can be modified by changing the Mo and Te constituents, and catalyst activity and selectivity can be improved by enhancing the number of V^{5+}-sites of the V–O–Mo and V–O–Te entities.

The results of López Nieto et al. [20] and Botella et al. [21] on catalyst fabrication suggest that H_6TeO_6 is superior to TeO_2 in the generation of Mo–V–Te–Nb catalysts for propane partial oxidation to AA. Our data reiterate that finding (see the results for the $A2^{\dagger}$ catalyst in Table 3). Nevertheless, we have demonstrated that with ultrasonic pretreatment, TeO_2 can be a suitable Te source for fabricating Mo–V–Te–Nb catalysts. The enhanced TeO_2 dispersion in a preparation medium can have a positive effect on (i) the precipitation of constituents during hydrothermal process, (ii) the elemental and phase composition of a catalyst, (iii) the dispersion of Te and Nb species, and (iv) the interaction of Nb species with Te–Mo and Te–V entities. It is noteworthy that the effectiveness of the ultrasonic treatment can vary among catalysts with different elemental compositions.

5. Conclusion

To summarize, we fabricated the Mo–V–Te–Nb MMOs using TeO_2 and H_6TeO_6 as Te sources through ultrasonic and hydrothermal treatments. The results demonstrate that the use of TeO_2 in catalyst preparation can be successful by enhancing the dispersion of TeO_2 in the preparation medium, and that the TeO_2-derived Mo–V–Te–Nb catalyst can be superior to the H_6TeO_6-derived counterpart in the partial oxidation of propane to AA. Over the TeO_2-derived A2 catalyst, an AA yield of 33.4 mol% and AA formation rate of 22.3 $\mu mol\, g^{-1}\, min^{-1}$ were recorded at 380 °C, which is comparable to the performance of the best MMO catalysts reported in the literature. The results of characterization show that the improved dispersion of TeO_2 in preparation media can result in (i) enhanced presence of the orthorhombic $Te_2M_{20}O_{57}$ (M = Mo, V, Nb) and hexagonal $Te_{0.33}MO_{3.33}$ (M = Mo, V, Nb) phases, (ii) surface enrichment of Te, (iii) increase in Mo–O–Te and V–O–Te entities, and (iv) better site isolation due to enhanced dispersion of Nb species. The redox and surface acidic properties of the catalysts fabricated with ultrasonic treatment also were found to be beneficial for the generation of AA.

Acknowledgments

Financial support was provided by Hong Kong Baptist University (FRG/06-07/I-08). The research activities conducted at NJU were financed by the NSFC (20673052) and JSNSF (BK2006112). X.J.Y. thanks Dr. Na Zhang for her kind help and fruitful discussions.

References

[1] S. Albonetti, F. Cavani, F. Trifiro, Catal. Rev. Sci. Eng. 38 (1996) 413.
[2] M.M. Lin, Appl. Catal. A 207 (2001) 1.
[3] G. Centi, F. Trifirò, J.R. Ebner, V.M. Franchetti, Chem. Rev. 88 (1988) 55.
[4] Y.F. Han, H.M. Wang, H. Cheng, J.F. Deng, Chem. Commun. (1999) 521.
[5] X.K. Li, W.J. Ji, J. Zhao, Z.B. Zhang, C.T. Au, Appl. Catal. A 306 (2006) 8.
[6] M.E. Davis, C.J. Dillon, J.H. Holles, J. Labinger, Angew. Chem. Inter. Ed. 41 (2002) 858.
[7] X.K. Li, J. Zhao, W.J. Ji, Z.B. Zhang, Y. Chen, C.T. Au, S. Han, H. Hibst, J. Catal. 237 (2006) 58.
[8] N. Mizuno, M. Tateishi, M. Iwamoto, Appl. Catal. A 128 (1995) 165.
[9] S.A. Holmesa, J. Al-Saeedi, V.V. Guliants, P. Boolchand, D. Georgiev, U. Hackler, E. Sobkow, Catal. Today 67 (2001) 403.
[10] T. Ushikubo, H. Nakamura, Y. Koyasu, S. Wajiki, U.S. patent 5 380 933 (1995), to Mitsubishi Chemical Company.
[11] M.M. Lin, Appl. Catal. A 250 (2003) 305.
[12] M.M. Lin, Appl. Catal. A 250 (2003) 287.
[13] H. Watanabe, Y. Koyasu, Appl. Catal. A 194 (2000) 479.
[14] P. Botella, J.M. López Nieto, B. Solsona, A. Mifsud, F. Marquez, J. Catal. 209 (2002) 445.
[15] K. Oshikara, T. Hisano, W. Ueda, Top. Catal. 15 (2001) 153.

[16] B.C. Zhu, H.B. Li, W.S. Yang, L.W. Lin, Catal. Today 93 (2004) 229.
[17] K. Asakura, K. Nakatani, T. Kubota, J. Catal. 194 (2000) 309.
[18] A.M. Gaffney, S. Chaturvedi, M.B. Clark Jr., S. Han, D. Lea, S.A. Rykov, J.G. Chen, J. Catal. 229 (2005) 12.
[19] P. Botella, B. Solsona, A. Martinez-Arias, J.M. Lopez-Nieto, Catal. Lett. 74 (2001) 149.
[20] J.M. López Nieto, P. Botella, B. Solsona, J.M. Oliver, Catal. Today 81 (2003) 87.
[21] P. Botella, P. Concepción, J.M. López Nieto, Y. Moreno, Catal. Today 99 (2005) 51.
[22] V.V. Guliants, R. Bhandari, H.H. Brongersma, A. Knoester, A.M. Gaffney, S. Han, J. Phys. Chem. B 109 (2005) 10234.
[23] E.K. Novakova, E.G. Derouane, J.C. Védrine, Catal. Lett. 83 (2002) 177.
[24] D. Vitry, Y. Morikawa, J.L. Dubois, W. Ueda, Appl. Catal. A 251 (2003) 411.
[25] T. Ushikubo, K. Oshima, A. Kayou, M. Hatano, Stud. Surf. Sci. Catal. 112 (1997) 473.
[26] M. Aouine, J.L. Dubois, J.M.M. Millet, Chem. Commun. (2001) 1180.
[27] M. Baca, A. Pigamo, J.L. Dubois, J.M.M. Millet, Top. Catal. 23 (2003) 39.
[28] J.M.M. Millet, H. Roussel, A. Pigamo, J.L. Dubois, J.C. Jumas, Appl. Catal. A 232 (2001) 77.
[29] M. Baca, M. Aouine, J.L. Dubois, J.M.M. Millet, J. Catal. 233 (2005) 234.
[30] P. Botella, J.M. López Nieto, B. Solsona, Catal. Lett. 78 (2002) 383.
[31] J.C. Védrine, E.K. Novakova, E.G. Derouane, Catal. Today 81 (2003) 247.
[32] P. Botella, J.M. López Nieto, B. Solsona, J. Mol. Catal. A 184 (2002) 335.
[33] M. Dieterle, G. Mestl, J. Jäger, Y. Uchida, H. Hibst, R. Schlögl, J. Mol. Catal. A 174 (2001) 169.
[34] N.C. Ramani, D.L. Sullivan, J.G. Ekerdt, J.-M. Jehng, I.E. Wachs, J. Catal. 176 (1998) 143.
[35] E. García-González, J.M. López Nieto, P. Botella, J.M. González-Calbet, Chem. Mater. 14 (2002) 4416.
[36] H. Hayashi, N. Shigemoto, S. Sugiyama, N. Masaoka, K. Saitoh, Catal. Lett. 19 (1993) 273.
[37] F.J.J.G. Janssen, J. Thermal Anal. 87 (1991) 1281.
[38] J.F. Moulder, W.F. Stickle, P.E. Sobol, K.D. Bomben, in: J. Chastain, R.C. King Jr. (Eds.), Handbook of X-Ray Photoelectron Spectroscopy, Physical Electronics, Inc., Minnesota, 1995, p. 111.
[39] A. Baiker, D. Monti, J. Catal. 91 (1985) 361.
[40] A. Kaddouri, C. Mazzocchia, E. Tempesti, Appl. Catal. A 180 (1999) 271.
[41] M. Ai, Catal. Today 42 (1998) 297.
[42] R.K. Grasselli, Top. Catal. 15 (2001) 93.
[43] W. Ueda, D. Vitry, T. Katou, Catal. Today 96 (2004) 235.
[44] W. Ueda, D. Vitry, T. Katou, Catal. Today 99 (2005) 43.
[45] R.K. Grasselli, Catal. Today 99 (2005) 23.
[46] D. Vitry, Y. Morikawa, J.L. Dubois, W. Ueda, Top. Catal. 23 (2003) 47.
[47] R.K. Grasselli, J.D. Burrington, D.J. Buttrey, P. Desanto Jr., C.G. Lugmair Jr., A.F. Volpe Jr., T. Weingand, Top. Catal. 23 (2003) 5.
[48] P. Botella, E. García-González, J.M. López Nieto, J.M. González-Calbet, Solid State Sci. 7 (2005) 507.
[49] R.M. Fong, X.J. Yang, H.Y. Zhu, X.D. Gu, W.J. Ji, Y. Chen, S. Han, H. Hibst, J. Mol. Catal. A 267 (2007) 245.